ANALYTICAL AND CFD INVESTIGATION OF TURBULENT DIFFUSION MODEL FOR PARTICLE DISPERSION AND DEPOSITION IN HORIZONTAL PIPE FLOW

Alamgir Hossain
Department of Mechanical Engineering, Military Institute of Science and Technology, Dhaka
Jamal Naser
Faculty of Engineering and Industrial Sciences, Swinburne University of Technology,
Hawthorn, VIC 3122, Australia
Corresponding email: aalamgir92@gmail.com

Abstract: *A 2D analytical turbulent diffusion model for particle dispersion and deposition at different heights across the pipe flow and circumferential deposition has been developed. This liquid-solid turbulent diffusion model presented in this paper has emanated from an existing gas-liquid turbulent diffusion model. Simultaneously a comprehensive 3D numerical investigation has been carried out to study the above making of multiphase mixture model available in Fluent 6.1. In both studies different particles sizes and densities were used. The deposition was studied as a function of particle diameter, density and fluid velocity. The deposition of particles, along the periphery of the wall and at different depths, was also investigated. Both studies showed that the deposition of heavier particles at the bottom of the pipe wall was found to be higher at lower velocities and lower at higher velocities. The lighter particles were found mostly suspended with homogeneous distribution. Smaller particles were also suspended with marginal higher concentration near the bottom of the wall. This marginal higher concentration of the smaller particles was found to be slightly pronounced for lower velocity. The larger particles clearly showed deposition near the bottom of the wall. These analogies of particles are well discussed with the ratio between free flight velocity and the gravitational settling velocity.*

Key Words: *Multiphase flow, turbulence diffusion, particle deposition, horizontal flow.*

INTRODUCTION

Particle dispersion and deposition in two-phase flows is very important, which has been well recognized in numerous fields of research and industry. Some examples are the transport of pollutants in the atmosphere and oceans, droplets in sprays and internal combustion engines, slurries in pipes, sediment transport in coastal areas, catalyst particles in riser flows, particles deposition in annular dispersed two-phase flow, fluidized beds, dust deposition and dust removal in clean rooms, etc. In most applications one is interested in how particles are transported by turbulent flows and where the particles eventually end up.

The motivation for this study is two-fold, first we are interested in the deposition of solid spherical particles with specific gravity 3.0 as it occurs in annular dispersed two phase flows in water supply networks. The dispersed phases of such flows consist of particles with diameters ranging from 5 μm to 100 μm. This study was also conducted for five different particle densities ranging from specific gravity (sg) 1.5 to 6.0 keeping the diameter constant at 10 μm. These sizes and densities ranges have been chosen in order to rationalize with present drinking water distribution networks [1]. These flows are rather complex and it is difficult to obtain detailed experimental data on the contribution to deposition in relation to particle size. The second point of interest of this study is to investigate the segregation of solid particles along the circumference of the pipe wall.

In order to obtain more insight into the process of particle dispersion and deposition 3D numerical CFD (Computational Fluid Dynamics) simulations were carried out at different Reynolds numbers. These above analytical studies have also been validated with the CFD investigation using the same particle parameters and the help of Multiphase mixture model using Fluent 6.1[2].

Smaller and lighter particles are driven by turbulence diffusivity, and can therefore, be found mostly suspended with homogeneous distribution; whereas in the case of larger and heavier particles gravitational force is predominant and particles clearly show deposition near the bottom of the wall. Finally, we have discussed the dispersion behavior of particles in turbulence pipe flow based on the velocity ratio (explained later).

TURBULENCE DIFFUSION MODEL

When faced with the task of modeling turbulent particles deposition, or any multiphase flow, two general approaches are possible. One is Lagrangian approach, usually known as a "trajectory model" [3], where the instantaneous motions of individual particles are tracked by solving their equations of motion. The trajectories of many particles (typically thousands) are realized

in order to form the average behavior of the particle-fluid system. The other is Eulerian, often called a "two-fluid" model, where the particles are treated as a continuous phase, in much the same way that a tracer fluid would be regarded in a binary mixture. The motion of the particulate phase is mathematically described by mass, momentum and energy conservation, similar to a fluid. In this study we followed the Eulerian approach, which is more suitable for re-suspension and/or re-deposition of particles than Lagrangian approach. In Lagrangian approach the particles are tracked through the fluid domain and their effects on the fluid flow are introduced through forces like drag. But the physical existence of the particles creating blockages or voidages is ignored. In order to study the behavior of particles in a turbulent flow field numerically, one needs a proper representation of turbulence itself.

The use of a cylindrical geometry in combination with a large range of particles (5 different sizes and 5 other different weighs of particles) makes this study of relevance for many practical applications and makes a comparison with the numerous experiments on particle deposition possible.

The deposition flux of particles at a certain circumferential angle in the pipe/tube has to be known [4, 5]. Except for very large particles (>100 □m), for which the motion is totally dominated by gravity and the particle's initial entrainment velocity [6-8], there is at present no theoretical analysis of this deposition flux in a two-dimensional geometry. Anderson and Russell[6] developed a semi-empirical expression to correlate deposition and entrainment fluxes, but only for the top half in the tube. The model used to derive this expression assumes that droplet deposition is caused by deterministic drop trajectories intersecting the liquid film. The work of [8] is an extension of the work of [7]. In both approaches no effect of turbulence was taken into account because only very large particles were considered. Laurinat et al.[5] proposed an empirical fit to a representative deposition flux profile measure by Anderson and Russell[6],

$$R_D(\phi) = k_D\left[1+10\exp\{2(\cos\phi-1)\}\right] \qquad (1)$$

where R_D is the deposition flux, k_D is a constant that has to be calculated from the entrainment of particles, and is the angle around the pipe circumference. Figure 1 gives a sketch of this correlation of Eq. (1) in units of k_D. The angle 0^o refers bottom and $\pm 180^o$ is the top wall of the pipe. Deposition is the highest at the bottom and the lowest at the top. In all horizontal annular flow models up till now a correlation like Eq. (1) or even a more simple deposition flux, not depending on the circumferential pipe angle, has been used.

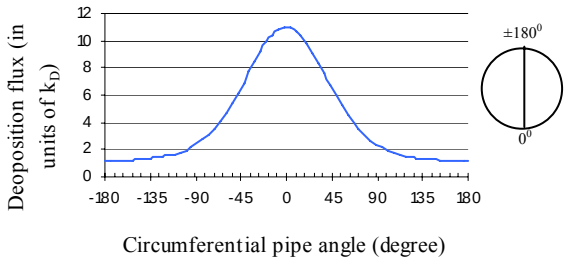

Figure 1. The deposition flux in a tube as a function of the circumferential angle in the pipe

The behavior of $R_D(\ )$ must depend on the fluid velocity. The difference between deposition at the bottom and top is expected to decrease with increasing fluid velocity due to increase of turbulence. In this study we investigate whether or not a more generalized form of this equation can be derived using a turbulent diffusion model[11] and thereafter compare with the CFD investigation.

Taylor[9] and then Friendlander and Johnstone[10] started at earlier days of Turbulent Diffusion Model. Taylor[9] introduced the concept of Turbulent Diffusion in a study of the spread of scalar properties like smoke, heat and soluble matter. Friendlander and Johnstone[10] used this concept for modeling a two-phase flow with particles. They also introduced the "diffusion/free-flight" concept (explained later) for particles depositing at a wall. In order to improve agreement with experimental data, different modifications of this concept were proposed in the course of time: varying free-flight distance from the wall; modifying free-flight velocity; particle diffusivity unequal to eddy diffusivity; changing concentration boundary condition at the free-flight distance[3].

In the field of particle deposition, the most recent contribution is the work of Binder and Hanratty[11], which is the starting point of this article. They considered the dispersion and deposition of particles in a two-dimensional horizontal rectangular channel by a convection/diffusion model. The diffusion part of this model represents the influence of turbulence and the convection part represents the influence of gravity on the particles. Particles are emitted from an instantaneous point source at the bottom of the channel with some initial entrainment velocity and can deposit at either of the perfectly absorbing boundaries. The particle diffusivity and the particle deterministic fall velocity are taken to be functions of the time that a particle has been in the flow field. The resulting convection/diffusion equation and the equation for the time-dependent deterministic velocity of the particles are solved numerically. One of their conclusions is that two dimensionless groups determine the resulting concentration profiles: the ratio of the time scale of the particle to the time scale of the flow, $_p/T_L$, and the Reynolds number based on the friction velocity, Re^*. $_p$ is

the particle relaxation time and T_L is the integral flow time scale.

The main differences between the method used in this paper and the approach of Binder and Hanratty[11] are two-fold. First, we assume the particle diffusion coefficient and the gravitational settling velocity to be stationary instead of time-dependent. This assumption has the great advantage that the one-dimensional problem can then be solved analytically, so that we find a general expression for the deposition flux independent of the exact quantitative modeling of the particle diffusion coefficient and the gravitational settling velocity. It furthermore has the advantage that an analytical two-dimensional deposition flux in a pipe can be calculated containing the relevant physical parameters of the problem that are hidden in empirical correlations like Eq. (1). Of course it has the disadvantage of not taking into account the fact that the particle deterministic velocity is generally time-dependent and that the particle diffusion coefficient is initially also time-dependent. Second, we explicitly include the inertial and crossing trajectories effects in the particle diffusion coefficient. Thus the particle diffusion coefficient is equal to the fluid diffusivity for $_p/T_L<1$, but smaller that the fluid diffusivity for $_p/T_L>1$ [12]. Binder and Hanratty[11] assumed the particle diffusion coefficient to be equal to the fluid diffusivity. They did not consider at all the crossing trajectories effect.

The rest of this paper is organized as follows. First, we will give a definition of the problem under consideration, specify the assumptions on which our model is based, and introduce the relevant length and time scales in the problem. Thereafter, we will specify a time-dependent, one-dimensional convection/diffusion problem, solve the accompanying equation analytically and use the solution to calculate one and two-dimensional deposition fluxes of particles with fluid-solid flow instead of gas/solid flow [12]. The two-dimensional deposition flux will be compared with the CFD investigation that has been simulated by using Multiphase Mixture Model in FLUENT 6.1[2]. At the end of this paper we will draw the most important conclusions of our analysis based on the ratio between free-flight velocity and settling velocity.

DEFINITION OF THE TURBULENT DIFFUSION PROBLEM

Particles are dispersed by turbulence and convected in between two infinite horizontal plates by gravity and they can deposit at the walls. The problem is sketched in Fig. 2. The streamwise turbulence is assumed to have little effect on the particle deposition at the walls, because the fluid mean velocity is dominant in the streamwise direction. It is assumed that particle can cross the boundary layers at the walls on their inertia. The time-dependent problem with perfectly absorbing walls is studied and we consider two initial conditions such as

- The initial conditions at which all the particles are homogeneously distributed on a pipe cross-section without having an initial radial velocity, and
- The initial condition of an instantaneous source at the bottom wall.

The initial condition is considered in the model at which all the particles are homogeneously distributed on a tube cross-section without having an initial radial velocity. The aim of this model is to predict from the turbulent diffusion model the relative concentration of particles and its dispersion.

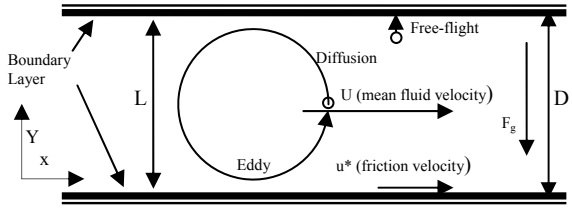

Figure 2. The diffusion/free-flight problem between two infinite horizontal plates

In the turbulent diffusion model the following assumptions are considered.

[1] Turbulent water flow in a horizontal pipe containing particle with a particle/fluid density ratios ranges from 1.5 to 6.0.

[2] Dilute particle suspension (volume fraction O (10^{-6}): one way coupling) without break-up and coalescence.

[3] Uniform and axial average fluid velocity (plug flow).

[4] Homogeneous turbulence up to the boundary layers.

[5] The particle mean free path is larger than the thickness of the boundary layer (so that there is a free flight of particles through the boundary layer to the wall) and the particle mean free path is smaller than the pipe diameter.

[6] Fick's law is valid, so that particles are in local equilibrium with the surrounding fluid, and a diffusion equation can be applied. For homogeneous turbulence this condition implies that the particle relaxation time must be much greater than the integral time scale of turbulence and much less than the particle diffusion time[14]. The motion of the particles is then statistically similar to Brownian motion.

[7] Particle free fall velocity, v_g, is considered stationary.

[8] Particle diameters lie between 5 and 100 μm, so Brownian motion can be ignored, and

[9] Particle motion is not fully dominated by gravity.

The assumptions of homogeneous turbulence and uniform, axial fluid velocity are more or less justified by assumption (viii). High inertia particles effectively see almost homogeneous turbulence (they do not respond much to gradients in the fluid r.m.s. velocity normal to the wall), and they will not respond much to variations in the mean flow of the fluid. These assumptions will be discussed more later in this paper.

The typical Eulerian eddy length scale is estimated 50 mm and the smallest scale of the turbulent structures (the Kolmogorov length scale,λ_K, which is approximately O(10^{-4}) shown in table 1) is calculated according to

$$\lambda_K \sim \left(\frac{\nu_f^3}{\varepsilon}\right)^{1/4} \tag{2}$$

where ν_f is the kinematic viscosity of the fluid, and ε the kinetic energy dissipation, given by

$$\varepsilon = k \cdot \frac{U^3}{L} \tag{3}$$

Table 1. Physical Properties of the system

Physical Characteristics	Description
Pipe diameter	4.72×10^{-1} m
Eulerian eddy length scale	5×10^{-2} m
Kolmogorov length scale	O(10^{-4})
Integral fluid time scale	O(10^{0})s
Particle relaxation time (d_p = 5μm)	O(10^{-6})s
Particle relaxation time (d_p = 100μm)	O(10^{-3})s

Velocity scale U is related to the friction velocity u^* and is approximately equal to one tenth of the average fluid velocity. Length scale L is approximately one tenth of the diameter of the pipe, and for a pipe proportional constant $k \approx 0.01$. These have been estimated according to Mols and Oliemans[12].

The integral time scale T_L of the fluid is given by

$$T_L = \int_{t_0}^{\infty} \frac{\langle v_f'(t) v_f'(t_0)\rangle}{\langle v_f'^2\rangle}\, dt \tag{4}$$

where v_f' is the fluctuating velocity of the fluid and t_0 some initial time. In a pipe flow, T_L will depend on the spatial position, but as homogeneous turbulence is assumed, T_L is taken to be constant. Approximately T_L can be calculated by

$$T_L \approx \frac{L}{U} \tag{5}$$

Large eddies are assumed to be dominant for the dispersion of particles the time scale T_L. However, there is in fact a whole range of time scales in turbulence. The particle relaxation time based on Stokes drag is equal to

$$\tau_p = \frac{1}{18}\frac{d_p^2}{\nu_f}\frac{(\rho_p - \rho_f)}{\rho_f} \tag{6}$$

with ν_f the kinematic viscosity of the fluid, and ρ_p and ρ_f the densities of, respectively, the particle and the fluid. For particle Reynolds numbers larger than one, the real relaxation time will be smaller due to the increased drag in the non-Stokes case. The ratio τ_p/T_L is called the Stokes number S and can be interpreted as a measure of the influence of particle inertia on the dispersion of the particles by fluid turbulence.

Three distinguish cases we can consider to lead to different responses on the turbulent fluctuations, different behavior in the boundary layer, and different concentration gradients. These are (i) the particle relaxation time is much smaller (S«1); (ii) of the same order of magnitude (S≈1); or (iii) much larger than the fluid integral time scale (S»1). For particle relaxation times much smaller than the fluid integral time scale (S«1), particles precisely follow the velocity fluctuations of the fluid, the deposition is delayed by the boundary layer and the deposition flux is low all around the pipe wall. For particle relaxation times of the same order of magnitude as the fluid integral time scale (S≈1), particles follow the turbulent fluctuations quite well, the effect of the boundary layer on the deposition is limited, and the deposition flux due to turbulence is high all around the pipe wall. For particle relaxation times much larger than the fluid integral time scale (S»1), the response to the turbulent fluctuations is slow, and the particles effectively see a randomly fluctuating velocity field. The deposition is not affected by the boundary layer, and the deposition flux is larger at the bottom and small at the top, due to gravity.

In this model we have assumed solid spherical particle in a turbulent water flow. For calculating Reynolds Number we have used a 0.1 m/s water velocity and pipe diameter 4.72×10^{-1} m, but to calculate length scale L, the only representative diameter of a particle, 100 μm, has been used.

MATHEMATICAL FORMULATION OF THE MODEL

The diffusion equation concept makes physically sensible when the relevant length scale over which the diffusion process is considered (here pipe diameter, D) is larger than the particle mean free path (defined in homogeneous turbulence), and the time of observation is larger than the mean free time (T_L). Following Swailes and Reeks[13] a particle mean free path can be

defined in a turbulent flow as the distance traveled by a particle in a time over which its motion is correlated. The particle mean free path l is then defined as

$$l = \sqrt{\langle v_p'^2 \rangle} T_p \tag{7}$$

with $\langle v_p'^2 \rangle$ is the particle mean square velocity and $T_P = T_L(1+S)$ the particle integral time scale. With increasing particle relaxation time, the particle r.m.s. velocity decreases, but the correlation time of the particle velocity increases more than the particle r.m.s. velocity decreases. Figure 3 gives the ratio between pipe diameter and mean free path, D/l, as a function of the particle diameter for two different velocities.

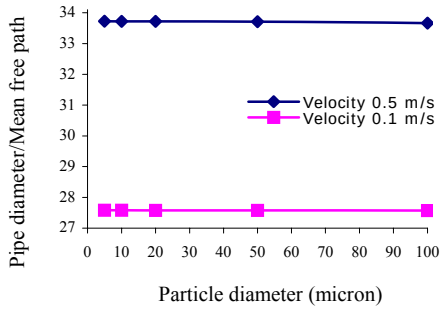

Figure 3. Ratio between pipe diameter and particle mean free path as a function of particle diameter for the velocity 0.1 and 0.5 m/s (D = 4.72310^{-1} m)

The largest particles that have been used in this calculation, 100μm, this ratio, D/l, is still larger than one, which supports assumption (5) in turbulent diffusion problem. The mean free path for very small particle are assumed to be determined by the Eulerian integral length scaled, which is 0.11 of the pipe diameter. D/l is then more than 27. However, in the limit of very large particles, the mean free path goes to infinity, and D/l goes to 0. The particle mean free path increases with increasing velocities.

The gradient diffusion model in inhomogeneous turbulence is must not valid unless $\tau_p^+ = \tau_p (u^*)^2 / \nu_f \ll 3$[14]. For the relaxation time larger than this limit, turbophoresis becomes important. Turbophoresis is the effect that particles migrate in inhomogeneous turbulence from a region of high turbulent velocity fluctuations to a region of low velocity fluctuations [14]. In the present model, however, it has been neglected, because homogeneous turbulence is assumed.

A time-dependent convection/diffusion equation in one spatial dimension is generally written as

$$\frac{\partial C(y,t)}{\partial t} = D_p \frac{\partial^2 C(y,t)}{\partial y^2} + v_g \frac{\partial C(y,t)}{\partial t} \tag{8}$$

where $C(y,t)$ is the particle concentration as a function of the spatial position y and time t. D_p is the particle diffusion coefficient and $v_g = g\tau_p$ the gravitational settling velocity of the particle. The first term on the right hand side is the diffusive term due to the influence of turbulence on the particles; the second term is the convective term due to the influence of gravity on the particles. Following Binder and Hanratty[11] we make variables dimensionless according to

$$y^+ \to \frac{y}{D};\ t^+ \to \frac{tu^*}{D};\ D_p{}^+ \to \frac{D_p}{u^* D};\quad v^+ \to \frac{v}{u^*};\ C^+ \to \frac{Cu^*}{R_e} \tag{9}$$

where R_e is the entrainment flux of the particles and u* is the friction velocity. The friction velocity is calculated by using the Blasius correlation for a smooth pipe

$$C_f = 0.0791 \cdot \mathrm{Re}_f^{-0.25} \tag{10}$$

where C_f is the friction coefficient, and Re_f is the fluid Reynolds number, which is defined as $V_f D/\nu_f$. V_f is the pipe average fluid velocity. From the friction coefficient the wall shear stress τ_s is calculated as

$$\tau_s = \tfrac{1}{2} \rho_f V_f^2 C_f \tag{11}$$

The wall shear stress is related to the friction velocity u^* by

$$u^* = \sqrt{\frac{\tau_s}{\rho_f}} \tag{12}$$

The one-dimensional convection/diffusion equation for the concentration of particles C^+ can then be written in the dimensionless form

$$\frac{1}{D_p^+} \frac{\partial C^+}{\partial t^+} = \frac{\partial^2 C^+}{\partial (y^+)^2} + P \frac{\partial C^+}{\partial y^+} \tag{13}$$

where Peclet number P is defined by

$$P := \frac{g\tau_p}{D_p} \cdot D \tag{14}$$

The Peclet number is the ratio of the convection term due to gravitational settling and the diffusion term due to turbulent diffusion. For Peclet number much smaller than one, diffusion term dominates. But Peclet numbers much larger than one, gravitational settling becomes dominant.

The particle diffusion coefficient D_p is related to the fluid diffusivity D_f by

$$\mathrm{D_p} = \gamma_{\mathrm{inert}} \gamma_{\mathrm{cross}} \mathrm{D_f} \tag{15}$$

where the fluid diffusivity is given by

$$D_f = \int_0^\infty \langle v_f'(0) v_f'(t) \rangle dt \approx \langle v_f'^2 \rangle \int e^{-\frac{1}{T_L}} dt = \langle v_f'^2 \rangle T_L \qquad (16)$$

The fluid mean square velocity $\langle v_f'^2 \rangle$ can be approximated by $(0.7 \times u^*)^2$ in the part of the pipe where turbulence is considered to be homogeneous [12]. In the absence of gravity, the ratio of particle and fluid diffusivity is governed by the ratio of particle relaxation time and fluid integral time scale and the inertial coefficient γ_{inert}, which can then be estimated from Mols and Oliemans[12] as

$$\gamma_{inert} = \frac{1}{\sqrt{1 + \tau_p / T_L}} \qquad (17)$$

The Equation (17) corresponds physically to a decreasing response of particles to fluid turbulence (in a wall bounded flow) if $\tau_p > T_L$. In the presence of a gravity field, a crossing trajectories effect generally has to be taken into account according to Csanady[15]. A particle falling through an eddy loses its velocity correlation more rapidly than a fluid element. Thus it sees a fluctuating velocity field that varies more rapidly in time than a fluid element. The velocity correlation of a fluid element is determined only by the decay of an eddy. The result is that the crossing trajectories effect leads to a decreased particle diffusivity. It is determined by the ratio between the fluid integral time scale T_L and the time spent by a particle within an eddy, L/v_g with L the Eulerian eddy length scale and $v_g = g\tau_p$ the gravitational settling velocity. The crossing trajectories coefficient γ_{cross} is then given by

$$\gamma_{cross} = \frac{1}{\sqrt{1 + \left(\frac{g \tau_p T_L}{L} \right)^2}} \qquad (18)$$

Figure 4 gives both inertial and crossing trajectories coefficient as a function of particle diameter for the velocity 0.1 m/s and 0.5 m/s. Figure 4 shows that for 50 μm particles the crossing trajectories effect can reduce particle diffusivity by about 8%, but for larger particle 100 μm this has been reduced by about 35% for an average fluid velocity 0.1 m/s. This effect is negligible for 50 μm particles and less than 5% for 100 μm particles at velocity 0.5 m/s. The crossing trajectories effect is much more important for the particle sizes larger than 50 μm.

Since the particle's mean free path is larger than the thickness of the boundary layer, a convection/diffusion equation is no longer valid for the particle behavior in the boundary layer. It is assumed that particles are projected towards the wall at the beginning of the boundary layer, leading to a free-flight flux $v \cdot C$, where, v has the dimensions of a velocity. The free-flight flux is then approximated by

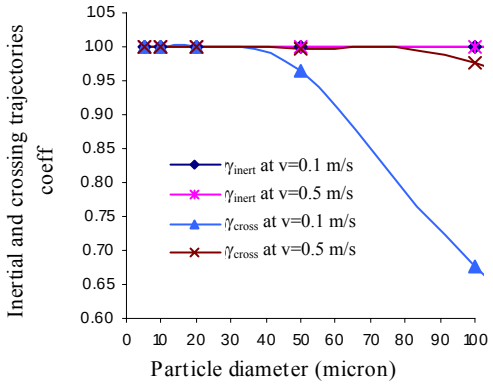

Figure 4. The inertial and crossing trajectories coefficients as a function of particle diameter for the velocity 0.1 and 0.5 m/s

$$v \cdot C = \int_0^\infty C \cdot vp(v) dv \qquad (19)$$

Since the particle's mean free path is larger than the thickness of the boundary layer, a convection/diffusion equation is no longer valid for the particle behavior in the boundary layer. It is assumed that particles are projected towards the wall at the beginning of the boundary layer, leading to a free-flight flux $v \cdot C$, where, v has the dimensions of a velocity. The free-flight flux is then approximated by

$$v \cdot C = \int_0^\infty C \cdot vp(v) dv \qquad (19)$$

where p(v) is the velocity distribution at the point from which the particles are projected in the direction of the wall. Integration is performed only over the particle velocities directed towards the wall. Following Binder and Hanratty[11], p(v) is assumed to be Gaussian. With this assumption Eq. (19) follows that

$$v \cdot C = \frac{1}{2} \sqrt{\frac{2}{\pi}} \sqrt{\langle v_p'^2 \rangle} \cdot C \qquad (20)$$

so that the free-flight velocity v is equal to

$$v = \frac{1}{2} \sqrt{\frac{2}{\pi}} \sqrt{\langle v_p'^2 \rangle} \qquad (21)$$

The particle mean square velocity is calculated from the ratio of velocity fluctuations between particle and fluid given in Hinze[16] in which the large density ratio between particle and fluid, leading to

$$\frac{\langle v_p'^2 \rangle}{\langle v_f'^2 \rangle} = \frac{1}{1+S} \qquad (22)$$

In the analysis, the crossing trajectories effect shown in Fig. 5 is fairly high especially at lower

velocity for particle sizes under consideration. The Eq. (22) is also used by Swailes and Reeks[13]. At the beginning of the boundary layers $\sqrt{\langle v_f'^2 \rangle} = 0.9 \cdot u^*$. Then it follows from Eq.s (21) and (22) that

$$v = \frac{1}{2}\sqrt{\frac{2}{\pi}}\sqrt{\frac{\langle v_f'^2 \rangle}{1+S}} \tag{23}$$

Binder and Hanratty[11] used the following empirical approximation:

$$\frac{\langle v_p'^2 \rangle}{\langle v_f'^2 \rangle} = \frac{1}{1+(0.7\tau_p / T_L)} \tag{24}$$

For Stokes relaxation time, this expression reduces to

$$\frac{\langle v_p'^2 \rangle}{\langle v_f'^2 \rangle} = \frac{1}{1+0.7 \cdot S} \tag{25}$$

having the same form as (22).

Now the boundary conditions can be derived by applying conservation of mass at the beginning of the boundary layer: the diffusive plus the gravitational flux towards the boundary layer $(D_p(\partial C)/(\partial y) + (v_g C)$ must be equal to the free-flight plus the gravitational flux from the boundary layer to the wall $(vC + v_g C)$. Assuming that the boundary layer is this enough to apply this condition exactly on the wall, the diffusion free-flight boundary condition ([11]) at the bottom wall ($y^+ = 0$):

$$D_p{}^+ \frac{\partial C^+}{\partial y^+} = v^+ C^+ \tag{26}$$

At the top wall ($y^+ = 1$), we have

$$-D_p{}^+ \frac{\partial C^+}{\partial y^+} = v^+ C^+ \tag{27}$$

A more theoretical discussion and justification of this type of boundary condition is given in Morse and Feshbach[17]. The ratio D_p/ν is of the order of the particle mean free path. Because the particles' mean free path is large compared to the length scale characterizing the variation in the particle concentration, $\partial C/\partial y$, there can be a finite concentration at the wall. For particles with S « 1 the particle mean free path vanishes at the wall, leading to the boundary condition, which normally represents perfect absorption, C = 0. To close the one-dimensional model, two initial conditions have been considered. The first initial condition is a uniform concentration:

$$C^+(t^+ = 0) = C_0 = 1 \tag{28}$$

The second initial condition is a delta source at the bottom wall:

$$C^+(t^+ = 0) = \delta(y^+) \tag{29}$$

Other initial conditions can be used without problems. This initial source at the bottom is the initial condition that was considered by Binder and Hanratty[11].

The mathematical formulation of the problem now consists of Eq. (13) with boundary conditions (Eqs (26) and (27)) and initial conditions (Eq. (28) or (29)).

ANALYTICAL SOLUTION OF THE ONE-DIMENSIONAL PROBLEM

Equation (13) with boundary conditions (Eqs (26) and (27)) and initial conditions (Eq. (28) or (29)) now can be solved analytically (by separation of variables) leading to a series solution for $C^+(y^+, t^+)$:

$$C^+(y^+, t^+) = \exp[-\tfrac{1}{2}Py^+]\sum_{n=0}\gamma_n[\cos(b_n y^+) + \beta_n \sin(b_n y^+)]\exp(-k_n{}^2 D_p{}^+ t^+) \tag{30}$$

The eigenvalues k_n are determined by the boundary conditions. We have defined the eigenvalues k_n in terms of b_n:

$$k_n^2 := b_n^2 + \left(\tfrac{1}{2}P\right)^2 \tag{31}$$

where b_n then satisfies the transcendental equation

$$\tan b_n = \frac{2\lambda b_n}{(a^2 - \lambda^2) + b_n^2} \tag{32}$$

λ is the dimensionless free-flight/diffusion ratio equal to vD/D_p. γ_n is used to satisfy the initial condition, and is given by

$$\gamma_n = \frac{\int_0^1 C^+(t=0)\exp(ay^+)(\cos b_n y^+ + \beta_n \sin b_n y^+)dy^+}{\int_0^1 \exp(2ay^+)(\cos b_n y^+ + \beta_n \sin b_n y^+)dy^+} \tag{33}$$

γ_n can be solved analytically. For $C^+(t=0)=\mathrm{d}(y^+)$ the numerator in Equation (33) is equal to 1.

Furthermore, we have defined

$$a: = -1/2P \tag{34}$$

and

$$\beta_n := \frac{\frac{vD}{D_p} + \frac{1}{2}P}{b_n} \tag{35}$$

Tables 2 and 3 give the properties of particles that are used in the Turbulent Diffusion Model. The first values given in each row are at v_f = 0.1 m/s, and the second values are given at v_f = 0.5 m/s.

Table 2. Properties of the different size particles with specific gravity 3.0 that are used in the Turbulent Diffusion Model (First values are for 0.1 m/s fluid velocity, second values are for 0.5 m/s fluid velocity)

d_p (μm)	τ_p	S	D/l	v_g (m/s)	v (m/s)	γ_{inert}	γ_{cross}	D_p (m^2/s)	P
5	2.78×10^{-6}	5.89×10^{-7}	27.6	2.73×10^{-5}	1.86×10^{-3}	1.0	1.000	6.21×10^{-5}	0.2
		2.94×10^{-6}	33.7		7.61×10^{-3}	1.0	1.000	2.08×10^{-4}	0.1
10	1.11×10^{-5}	2.35×10^{-6}	27.6	1.09×10^{-4}	1.86×10^{-3}	1.0	1.000	6.21×10^{-5}	0.8
		1.18×10^{-5}	33.7		7.61×10^{-3}	1.0	1.000	2.08×10^{-4}	0.2
20	4.44×10^{-5}	9.42×10^{-6}	27.6	4.36×10^{-4}	1.86×10^{-3}	1.0	0.999	6.20×10^{-5}	3.3
		4.71×10^{-5}	33.7		7.61×10^{-3}	1.0	1.000	2.07×10^{-4}	1.0
50	2.78×10^{-4}	5.89×10^{-5}	27.6	2.73×10^{-3}	1.86×10^{-3}	1.0	0.965	5.99×10^{-5}	21.5
		2.94×10^{-4}	33.7		7.60×10^{-3}	1.0	0.999	2.07×10^{-4}	6.2
100	1.11×10^{-3}	2.35×10^{-4}	27.6	1.09×10^{-2}	1.86×10^{-3}	1.0	0.676	4.19×10^{-5}	122.6
		1.18×10^{-3}	33.7		7.60×10^{-3}	1.0	0.977	2.03×10^{-4}	25.4

Table 3. Properties of the different weighted particles with diameter 10 μm that are used in the Turbulent Diffusion Model (First values are for 0.1 m/s fluid velocity, second values are for 0.5m/s fluid velocity)

Sg	τ_p	S	D/l	v_g (m/s)	v (m/s)	γ_{inert}	γ_{cross}	D_p (m^2/s)	P
1.5	2.78×10^{-6}	5.89×10^{-7}	27.6	2.73×10^{-5}	1.86×10^{-3}	1.0	1.000	6.21×10^{-5}	0.2
		2.94×10^{-6}	33.7		7.61×10^{-3}	1.0	1.000	2.08×10^{-4}	0.1
2.5	8.33×10^{-6}	1.77×10^{-6}	27.6	8.18×10^{-5}	1.86×10^{-3}	1.0	1.000	6.21×10^{-5}	0.6
		8.83×10^{-6}	33.7		7.61×10^{-3}	1.0	1.000	2.08×10^{-4}	0.2
4.0	1.67×10^{-5}	3.53×10^{-6}	27.6	1.64×10^{-4}	1.86×10^{-3}	1.0	1.000	6.20×10^{-5}	1.2
		1.77×10^{-5}	33.7		7.61×10^{-3}	1.0	1.000	2.08×10^{-4}	0.4
5.0	2.22×10^{-5}	4.71×10^{-6}	27.6	2.18×10^{-4}	1.86×10^{-3}	1.0	1.000	6.20×10^{-5}	1.7
		2.35×10^{-5}	33.7		7.61×10^{-3}	1.0	1.000	2.07×10^{-4}	0.5
6.0	2.78×10^{-5}	5.89×10^{-6}	27.6	2.73×10^{-4}	1.86×10^{-3}	1.0	1.000	6.20×10^{-5}	2.1
		2.94×10^{-5}	33.7		7.61×10^{-3}	1.0	1.000	2.07×10^{-4}	0.6

The solution $C^+(y^+, t^+)$ given by Eq. (30) depends on three physical parameters: the Peclet number P, the dimensionless free-flight/diffusion ratio vD/D_p (determining the boundary conditions), and the initial condition $C^+(t = 0) = C_0$.

The deposition flux, R_D, given by the sum (for the bottom wall) or the difference (for the top wall) of the free-flight flux and the gravitational settling flux:

$$R_D = (v \pm v_g)C \tag{36}$$

For $v_g > v$, the particle concentration at the top is equal to 0. The ratio $D_{rel}(t^+)$ of deposition fluxes at the top and at the bottom then follows straight from the solution for the concentration ([12]) and Eq. (24):

$$D_{rel}(t^+) = \frac{v \pm v_g}{v + v_g}\exp\left[-\frac{1}{2}P\right] \frac{\sum_{n=0}^{\infty}\gamma_n\{\cos(b_n) + \beta_n \sin(b_n)\}\exp\left(-k_n^2 D_p^+ t^+\right)}{\sum_{n=0}^{\infty}\gamma_n \exp\left(-k_n^2 D_p^+ t^+\right)} \tag{37}$$

Particles can deposit at the top wall only when free-flight velocities are much larger than the gravitational settling velocity. For infinity time ($t \to \infty$), when the initial condition does not affect the solution anymore, then Eq. (37) follows that

$$D_{rel} = \frac{|v - v_g|}{v + v_g}\exp\left[-\frac{1}{2}P\right] \tag{38}$$

Table 4 shows the velocity ratio (ratio of gravitational settling velocity, v_g, to free-flight velocity, v) for different particles for the velocity of 0.1 and 0.5 m/s. When v_g>0.25v, the particles will be settled at the bottom wall by the influence of gravitational force; whereas, if v_g<0.25v, particles remain suspended mostly with homogenous distribution across the pipe for turbulence diffusion. Table 4 shows that in between 5 and 20 μm particles have free flight velocities, *v*, less than one fourth of its gravitational settling velocities so these particles can be found at the top of the pipe (Figs 5-6).

Table 4. Gravitational settling velocity (v_g) and its ratio to free-flight velocity (v)

Particle Diameter d_p (μm)	**sg**	**Settling Velocity v_g (m/s)**	**Velocity Ratio = v_g/v**	
			0.1 m/s	0.5 m/s
5	3.0	4.09×10^{-05}	0.02	0.01
10		1.64×10^{-04}	0.09	0.02
20		6.54×10^{-04}	0.35	0.09
50		4.09×10^{-03}	2.21	0.55
100		1.64×10^{-02}	8.79	2.15
10	1.5	8.18×10^{-05}	0.04	0.01
	2.5	1.36×10^{-04}	0.07	0.02
	4.0	2.18×10^{-04}	0.12	0.03
	5.0	2.73×10^{-04}	0.15	0.04
	6.0	3.27×10^{-04}	0.20	0.05

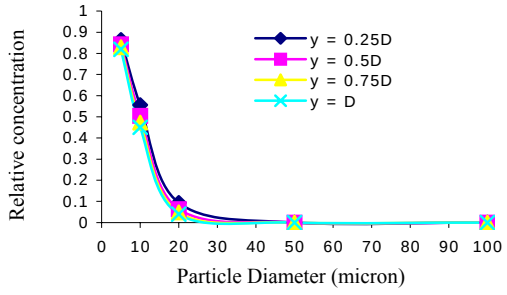

Figure 5a. Relative concentration of particles for different height as a function of particle diameter for the velocity 0.1 m/s

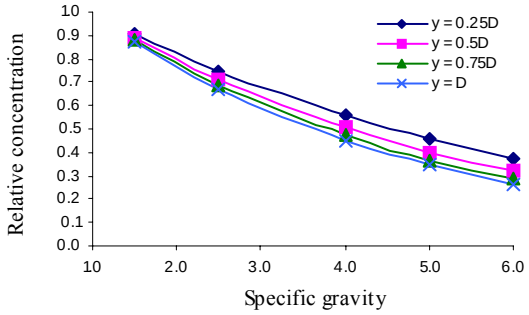

Figure 5b. Relative concentration of particles for different height as a function of specific gravity for the particle of 10 μm at velocity 0.1 m/s

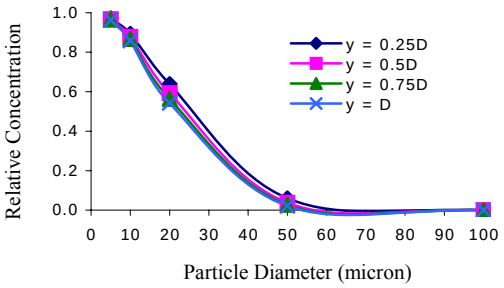

Figure 6a. Relative concentration of particles for different height as a function of particle diameter for the velocity 0.5 m/s

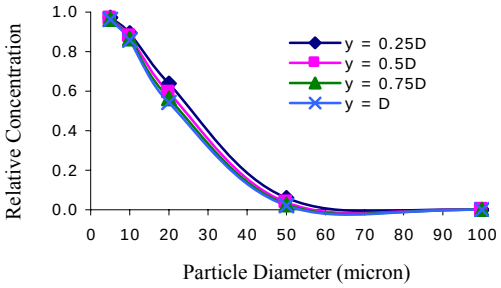

Figure 6b. Relative concentration of particles for different height as a function of specific gravity for the particle of 10 μm at velocity 0.5 m/s

Figures 5a and 6a show the relative concentration plotted as a function of particle diameter for different heights of 0.25D, 0.5D, 0.75D, and 1D from the bottom wall of the pipe. Relative concentration is a dimensionless parameter, which represents the ratio between local particle concentration at any heights and that of at bottom of the pipe wall. Particles larger than 25 μm are not able to reach at top wall for the velocity 0.1 m/s but for higher 0.5 m/s (Fig. 6a) particles larger than 50 μm do not reach to top wall. Both cases v_g>0.25*v* (Table 4) and particle are settled at the bottom by the influence of gravitational force (figs 5a and 6a). In Figs. 5b and 6b the relative concentration are plotted as a function of particle density, where most of the particles remain suspended due to v_g<0.25*v* (Table 4).

In fig. 7 the relative concentration is plotted as a function of particle diameter for the pipe diameter D = 4.72×10^{-1} m (top wall). Note that the curve for velocity 0.5 m/s lies much above the one for velocity 0.1 m/s in the region 5 μm < d_p < 50 μm. This is due to two effects, which compensate each other to a certain extent. For a higher velocity, the correlation time T_L decreases (Table 3), leading to a larger Stokes number, and a decreasing of particle diffusivity as a result of inertial effect, which is very minor shown in Fig. 5. On the other hand, the particle diffusivity increases due to the increasing

fluid diffusivity. The latter increases more than the former decreases, so that, according to Eq. (18), the net particle diffusivity increases slightly going to higher velocity. Relative concentration for the velocity 0.1 m/s drops to zero for the particle 50 μm and larger whereas it happens for the particle size larger than 55 μm when fluid velocity 0.5 m/s.

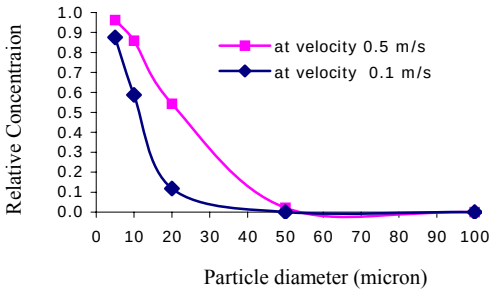

Figure 7. Comparison of the relative concentration of particles between top and bottom of the pipe as a function of the particle diameter at velocity 0.1 and 0.5 m/s

EXTENSION TO A TWO-DIMENSIONAL DEPOSITION FLUX COMPARISON WITH A SEMI EMPIRICAL CORRELATION

Paras and Karabelas[18] found in their experiment with a horizontal annular dispersed gas-liquid flow with more or less constant particle distribution. Using this experimental result as an extra assumption, Mols and Oliemans[12] proposed a one-dimensional model, which can be extended to a quasi two-dimensional model by substituting

$$y^+ = \frac{y}{D} \to \frac{1}{D}\cdot\left(\frac{1}{2}D(1-\cos\phi)\right) = \frac{1}{2}(1-\cos\phi) \quad \text{in}$$

$R_D{}^+(\phi, t^+) = (v^+ + v_g{}^+)C^+(y^+, t^+)$, where $C^+(y^+, t^+)$ is given in Eq. (30). D is the diameter of the pipe. Furthermore, we substitute $v_g{}^+ \to v_g{}^+\cos\phi$ in the expression for the deposition flux. This leads to

$$R_D{}^+(\phi,t^+) = (v^+ + v_g{}^+\cos\phi)\exp\left[\frac{1}{2}P(\cos\phi-1)\right]$$
$$\cdot \sum_{n=0}^{\infty}\gamma_n\left[\cos\left(\frac{1}{2}b_n(1-\cos\phi)\right) + \beta_n\sin\left(\frac{1}{2}b_n(1-\cos\phi)\right)\right]\exp\left(k_n{}^2 D_p{}^+ t^+\right) \quad (39)$$

Since we have assumed turbulence to be homogeneous, the free-flight velocity is independent of ϕ. The Eq. (39) is not of a genuine physical origin for our two-dimensional case. Therefore, the results of Eq. (39) leads to a local minimum at ϕ = 0 and local maxima at ϕ values slightly larger than 0. This is an artificial effect. As the series term in Eq. (39) is a term depending on the initial entrainment condition (via γ_n), Mols and Oliemans[12] proposed to write if for the stationary case as some unknown constant C_E, to be determined by the initial entrainment condition. C_E will generally differ for different particle relaxation times. The final result for the two-dimensional deposition flux that follows from their analysis can then be written as

$$R_D(\phi,\tau_p) = k_D(\phi,\tau_p)\cdot\exp\left[\tfrac{1}{4}P(\cos\phi-1)\right] \quad (40)$$

where the local deposition constant $k_D(\phi,\tau_p)$ is defined as

$$k_D(\phi,\tau_p) = C_E(\tau_p)\cdot(v + v_g\cos\phi) \quad (41)$$

having the dimension of velocity. The constant C_E can be determined from the fact that in a fully developed annular liquid-solid flow the total entrainment flux equals the total deposition flux ([12]):

$$\int_0^{\pi} R_E(\phi,\tau_p)d\phi = \int_0^{\pi} R_D(\phi,\tau_p)d\phi \quad (42)$$

From Eq.s (40), (41), and (42) it follows that

$$C_E(\tau_p) = \frac{\int_0^{\pi} R_E(\phi,\tau_p)d\phi}{\int_0^{\pi}\left[v + v_g\cos\phi\right]\exp\left[\tfrac{1}{4}P(\cos\phi-1)\right]d\phi} \quad (43)$$

From Eq.s (40 and 41) we can have deposition flux normalized by C_E:

$$\frac{R_D}{C_E} = (v + v_g\cos\phi)\cdot\exp\left[\tfrac{1}{4}P(\cos\phi-1)\right] \quad (44)$$

In Figs 8a and 8b, we have plotted the deposition flux normalized by C_E (Eq. (44)) for two velocities as a function of the circumferential pipe angle for six different particle sizes (5, 10, 20, 50, and 100 μm particles). Although we have plotted these curves in one figure, we recall that C_E is generally different for different particle relaxation times. This means that for each particle relaxation time the curves in Figs. 8a and 8b have to be multiplied by a different multiplication factor C_E with respect to the horizontal axis.

Figures 8a and 8b show the deposition flux plotted as a function of circumferential pipe angle for different particles. Figure 8b shows that 50 μm particles are just able to deposit at the bottom of the pipe wall, 100 μm particles can only deposit up to one third of the pipe wall circumference. In Figure 8a, the smaller particles exhibit broader deposition with minimum scale. However, depending on weights all particles are more or less disperse everywhere across the pipe with broader minimum scale deposition shown in Fig. 8b. For the lighter and smaller particles, the influence of gravity becomes less, which results particles deposit more

and more uniformly around the pipe circumference. In both cases the deposition flux increases at higher velocity. The width of the deposition curves is mainly determined by $\frac{1}{4}$P. the width decreases if the Peclet number increases. The Peclet number increases if the acceleration of gravity and/or the radius of the pipe increase, and/or if the particle diffusion coefficient decreases [12]. In the limit P→0 the influence of gravity is negligible and $R_D(\phi)$ becomes a constant independent of ϕ. However in the limit P→∞ the influence of gravity is infinite, and there can only be deposition at the bottom of the pipe[12].

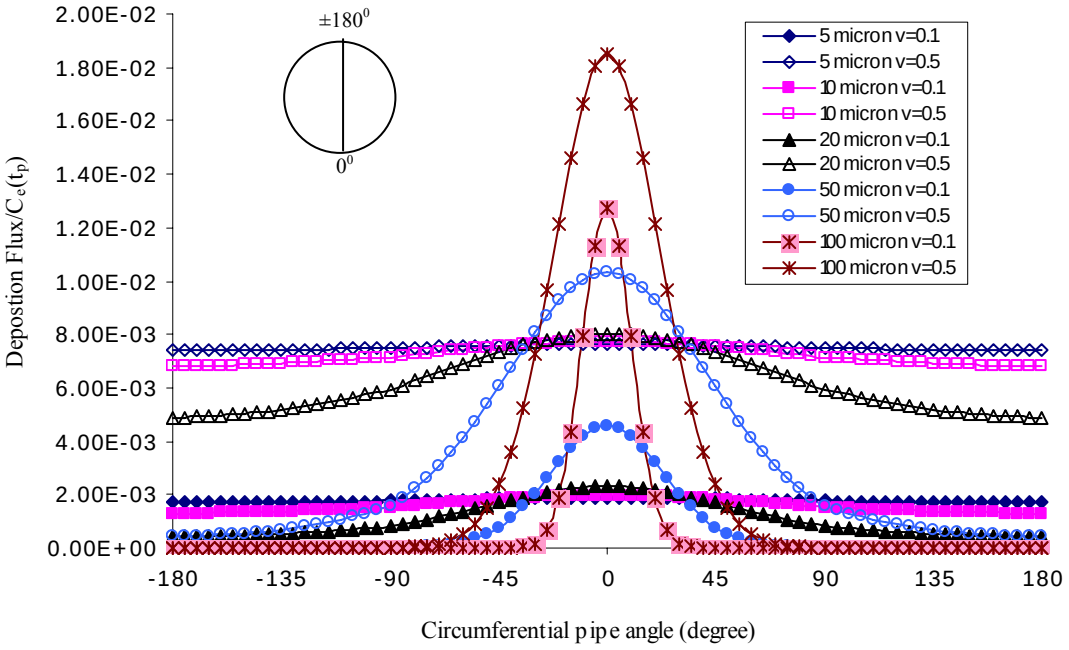

Figure 8a. Deposition flux normalized by $C_E(\tau_p)$ vs circumferential pipe angle for five different particle sizes for the velocity 0.1 and 0.5 m/s

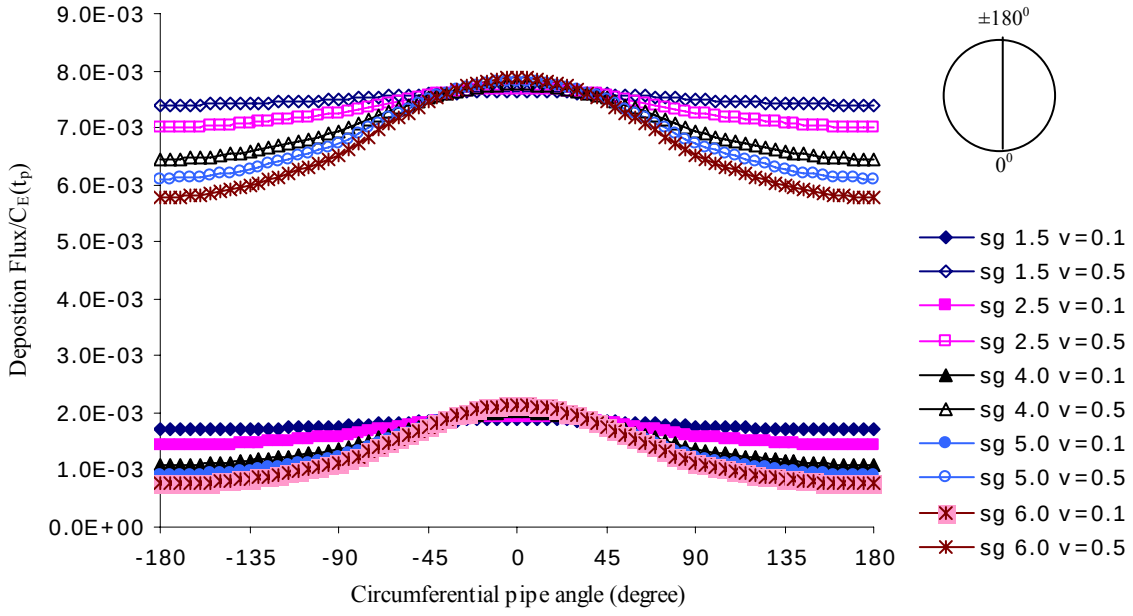

Figure 8b. Deposition flux normalized by $C_E(\tau_p)$ vs circumferential pipe angle for five different particle densities for the velocity 0.1 and 0.5 m/s

CFD INVESTIGATION AND RESULTS COMPARISON

A comprehensive 3D numerical simulation has been carried out to compare with the analytical model mentioned above. Multiphase Mixture Model available in Fluent 6.1[2] was used for predicting the liquid and solid phases. The model proposed by Spalart and Allmaras[19] was used for calculating the turbulence parameters. Table 5 shows the physical and hydraulic parameters of the system that has been used for CFD investigation.

Table 5. Properties of the different weighted particles with diameter 10 μm (First values are for 0.1 m/s fluid velocity, second values are for 0.5m/s fluid velocity)

Fluid velocity	Free-flight velocity (v)
0.1 m/s	1.82×10^{-3} m/s
0.5 m/s	7.61×10^{-3} m/s

Figures 9a-9d show analytical and simulated relative concentration plotted as a function of particle diameter for different height of 0.25D, 0.5D, 0.75D, and 1D from the bottom wall of the pipe. The figures show that the analytical relative concentration deviates between higher and lower velocity for the smaller particle.

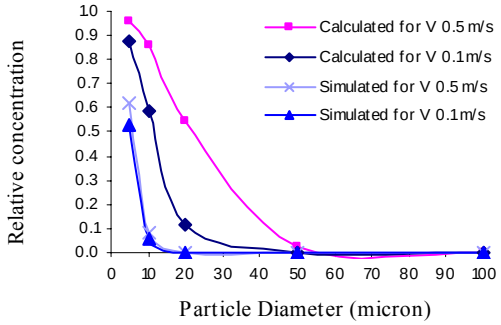

Figure 9a. Comparison of analytical and simulated relative concentration as a function of particle diameter at the top of pipe for velocity of 0.1 and 0.5 m/s

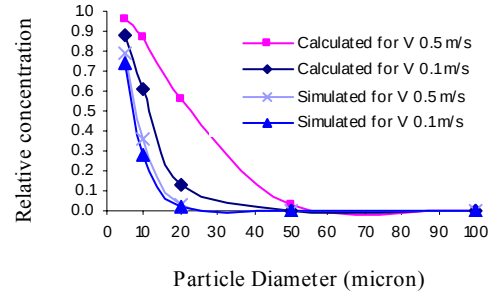

Figure 9b. Comparison of analytical and simulated relative concentration as a function of particle diameter at the height of y = 0.75D from bottom for velocity of 0.1 and 0.5 m/s

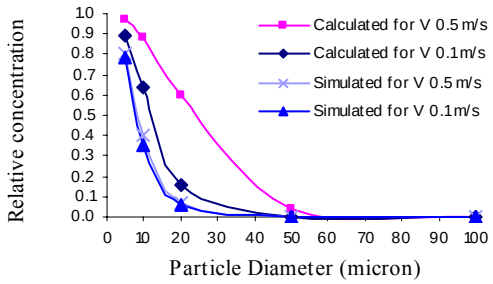

Figure 9c. Comparison of analytical and simulated relative concentration as a function of particle diameter at the center of pipe for velocity of 0.1 and 0.5 m/s

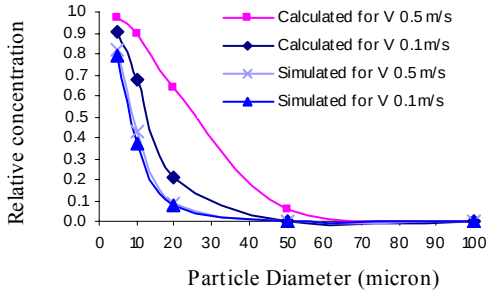

Figure 9d. Comparison of analytical and simulated relative concentration as a function of particle diameter at the height of y = 0.25D from bottom for velocity of 0.1 and 0.5 m/s

At higher velocity analytical relative concentration is also higher than that of lower velocity. This is because of turbulence diffusion, which increases due to velocity increase. However, simulated relative concentration shows no difference for larger particles, which are governed by the gravitational forces.

Figures 10a-10d show analytical and simulated relative concentration plotted as a function of particle specific gravity for different height of 0.25D, 0.5D, 0.75D, and 1D from the bottom wall of the pipe. Most of the particles remain suspended everywhere across the pipe. For the same size of particles, density does not affect for their deposition much. This can be easily explained when we considered the ratio between v_g and v. Table 4 shows that the free flight velocity is much more higher than the gravitational settling velocity results the turbulence diffusivity over rules on body force, which may be the cause of suspension and/or dispersion of particles.

Figures 9 (a-d) and 10 (a-d) show that the analytical relative concentration exhibits higher values than that of CFD simulated concentration. This may be explained by particle interaction[20] and 3D effect, which are considered for CFD simulation, cause higher deposition for CFD simulation whereas particle interaction has ignored for analytical model.

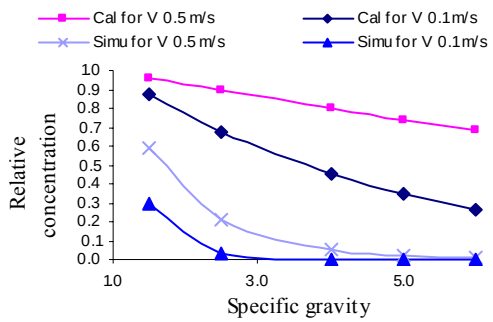

Figure 10a. Comparison of analytical and simulated relative concentration as a function of particle weight at the top of the pipe for velocity of 0.1 and 0.5 m/s

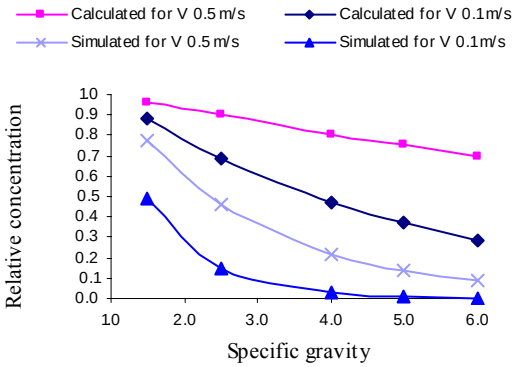

Figure 10b. Comparison of analytical and simulated relative concentration as a function of particle weight at the height of y = 0.75D from bottom for velocity of 0.1 and 0.5 m/s

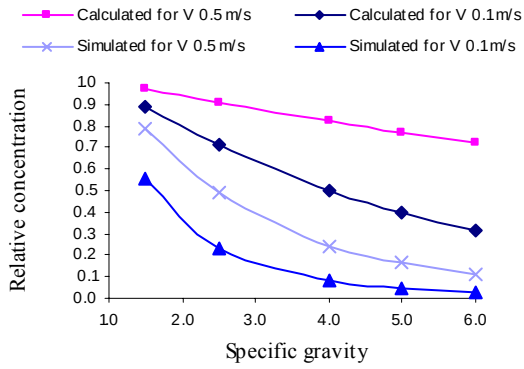

Figure 10c. Comparison of analytical and simulated relative concentration as a function of particle weight at the center of the pipe for velocity of 0.1 and 0.5 m/s

Local deposition rates along the pipe circumference can be obtained from the simulation. Figures 11a-11b show typical circumferential distributions of particles volume fraction for the velocity of 0.1 and 0.5 m/s. Most of the profiles exhibit a smooth variation with the maximum deposition at the bottom of the pipe. The overall qualitative trend of the present numerical results are similar to those of the experimental data of Anderson & Russell[6] and simulated results of Mols and Oliemans[12]. However, the present result obtained for Liquid-Solid system can not be compared quantitatively with those of Mols and Oliemans[12] and Anderson and Russell[6], which were obtained for Gas-Solid system.

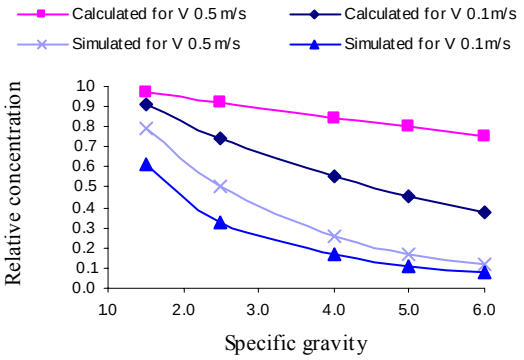

Figure 10d. Comparison of analytical and simulated relative concentration as a function of particle weight at the height of y = 0.25D from bottom wall for velocity of 0.1 and 0.5 m/s

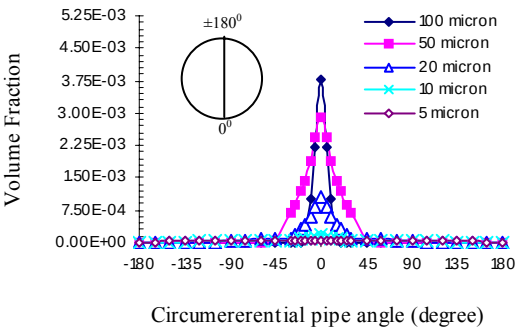

Figure 11a. Circumferential deposition as a function of circumferential pipe angles for five different particle sizes for the velocity 0.1 m/s

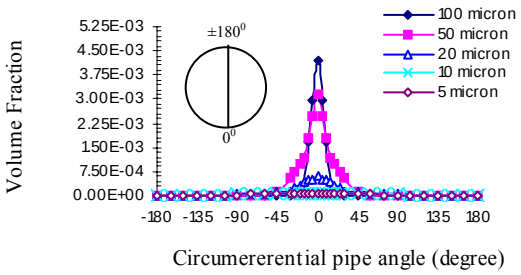

Figure 11b. Circumferential deposition as a function of circumferential pipe angles for five different particle sizes for the velocity 0.5 m/s

Figures 11a-11d show the volume fraction of different size particles (5, 10, 20, 50, and 100 μm, specific gravity 3.0) plotted as a function of the circumferential pipe angles. Particles ≥ 20 μm show greater concentration near the bottom wall of

the pipe. The smaller size particles remain suspended and uniformly dispersed due to heavily influences of turbulence diffusion, which nullify the gravity forces.

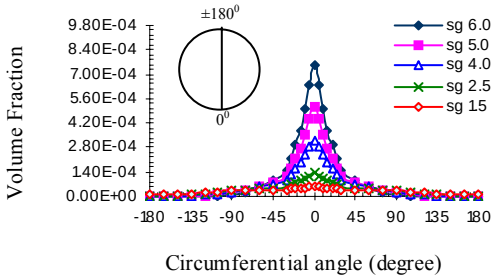

Figure 11c. Circumferential deposition as a function of circumferential pipe angles for five different particle densities for the velocity 0.1 m/s

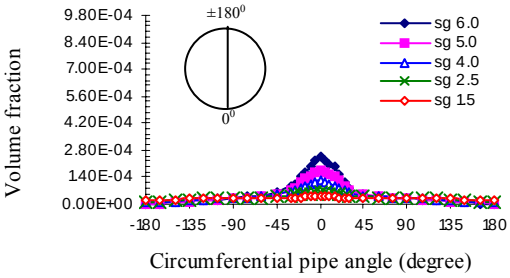

Figure 11d. Circumferential deposition as a function of circumferential pipe angles for five different particle densities for the velocity 0.5 m/s

The influence of the Reynolds number on the deposition on the pipe wall is also shown in the Figs. 11a-11b. For the smaller particle sizes the influence of the velocity change will be larger (also Figs. 10a-10d). This is an effect, which can be expected on the basis of the fact that for smaller particles (v_g<0.25v) the influence of turbulent diffusion is relatively large in comparison with the influence of gravity. Therefore, the particles ≤ 20 μm (v_g<0.25v) have not been influenced by gravity and show higher deposition at the bottom at lower velocity. The uniformity of dispersion increases with the flow velocity. Larger particles (v_g>0.25v), which are influenced by the gravity, settle more for higher velocity. This phenomenon has not been observed for the analytical calculation. The influence of the Reynolds number on the deposition of 10 μm particle with different densities is shown in the Figs. 11c-11d. These figures show the volume fraction of different density particles (1.5, 2.5, 4.0, 5.0, and 6.0 gm/cm^3, diameter 10 μm) plotted as a function of the circumferential pipe angles. The particles, which exhibit v_g<0.25v (Table 4), are less sensitive to gravity force and strongly influenced by the diffusivity of the fluid, which increases due to increase of velocity[12]. Table 4 shows that the ratio of free flight velocities to settling velocity for 0.1 m/s is relatively higher than that for 0.5 m/s. This resulted in higher concentration of heavier particles near the bottom of the pipe for lower velocity 0.1 m/s (Fig. 11c) as compared to that of 0.5 m/s (Fig. 11d).

Froude number also influences the deposition flux shown in Fig. 8 Fig. 11. The smaller and lighter particles are influenced more due to change in the Froude number (Table 3). Again, this is an effect which can be expected on the basis of the fact that for smaller and lighter particles the influence of turbulent diffusion is relatively large in comparison with influence of gravity. For a larger Froude number the deposition flux at a certain ϕ is larger. For the smaller and lighter particles, this effect decreases with increasing particle relaxation time. For the 100 μm particles this effect is very little due to the fact that for larger fluid velocities the effect of an increasing fluid diffusion coefficient is partly compensated by a decreasing inertial coefficient (see Table 1 and 2).

CONCLUSIONS

This paper investigated the effect of particle size, particle density and Reynolds number on the deposition and dispersion in a horizontal pipe for both analytical and CFD simulation. The larger particles, which exhibit the velocity ratio of gravitational settling velocity to free flight velocity (Table 4) more than 0.25, in general, are influenced by gravity, and show a tendency of settlement. But smaller particles, which exhibit the ratio of gravitational settling velocity to free flight velocity, less than 0.25, are influenced by turbulent diffusivity and are dispersed more or less uniformly across the cross section of the pipe. In the analytical model, homogeneous turbulence and uniform axial velocity through out the pipe flow have been considered, which may be the cause of slightly higher concentration in compare to CFD simulation in which particle interaction forces also included. For smaller and lighter particles the influence of turbulent diffusion is relatively large in comparison with influence of gravity.

CFD simulation results and analytical results differ slightly shown in this paper. This is because of the assumptions on which this analytical Turbulent Diffusion Model is based. The average fluid velocity will not be uniform over the whole cross-section of the pipe and turbulence will also be inhomogeneous close to the wall. The turbulent fluctuations here become too small to support the motion of these particles to the wall. Whereas, in CFD simulation velocity gradient and inhomogeneous turbulence near wall are incorporated into the model[2], which exhibit slight difference in relative particles concentration.

REFERENCES

[1] Grainger, C., Wu, J., Nguyen, B. V., Ryan, G., Jayanratne, A., and Mathes, P., 2003, "Part 1: Settling, Re-Suspension and Transport." CRC, CFC, Melbourne, Australia.

[2] FLUENT. FLUENT INC. 2001. USA.

[3] Kallio, G. A. and Reeks, M. W., 1989, "A Numerical simulation of particle deposition in turbulent boundary layers." International Journal of Multiphase Flow, 15(3), 433-446.

[4] Fukano, T. and Ousaka, A., 1989, "Prediction of the circumferential distribution of film thickness in horizontal and near-horizontal gas-liquid annular flows." International Journal of Multiphase Flow, 15, 403-419.

[5] Laurinat, J. E., Hanratty, T. J., and Jepson, W. P., 1985, "Film thickness distribution for gas-liquid annular flow in a horizontal pipe." Phys. Chem. Hydrodynamics, 6, 179-195.

[6] Anderson, R. J. and Russell, T. W. F., 1970, "Circumferential variation of interchange in horizontal annular two-phase flow." Ind. Engg. Chem. Fundam., 9, 340.

[7] Anderson, R. J. and Russell, T. W. F., 1970b, "Film formation in two-phase annular flow." AIChE Journal, 14, 626-633.

[8] James, P. W., Wilkes, N. S., Conkie, W., and Burnes, A., 1987, "Developments in the modelling of horizontal annular two-phase flow." International Journal of Multiphase Flow, 13, 173-198.

[9] Taylor, G. I., 1921, "Diffusion by continuous movements." Proceedings of the London Mathematical Society, 196-212.

[10] Friendlander, S. K. and Johnstone, H. F., 1957, "Deposition of suspended particles from turbulent gas streams." Industrial and Engineering Chemistry, 49, 1151.

[11] Binder, J. L. and Hanratty, T. J., 1992, "Use of Lagrangian method to describe drop deposition and distribution in horizontal gas-liquid annular flows." International Journal of Multiphase Flow, 18, 403-419.

[12] Mols, B. and Oliemans, R. V. A., 1998, "A Turbulent diffusion model for particle dispersion and deposition in horizontal tube flow." International Journal of Multiphase Flow, 24(1), 55-75.

[13] Swailes, D. C. and Reeks, M. W., 1994, "Particle deposition from a turbulent flow. I. A steady-state model for high inertia particles." Physics of Fluids, 6(10), 3392.

[14] Reeks, M. W., 1983, "The transport of discrete particles in inhomogeneous turbulence." Journal of Aerosol Science, 14, 729-739.

[15] Csanady, G. T., 1963, "Turbulent diffusion of heavy particles in the atmosphere." Journal of Atmospheric Science, 20, 201-208.

[16] Hinze, J. O., 1975, Turbulence, McGraw-Hill.

[17] Morse, P. M. and Feshbach, H., 1953, Methods of Theoretical Physics, McGraw-Hill, New York, USA.

[18] Parash, S. V. and Karabelas, A. J., 1991, "Droplet entrainment and deposition in horizontal annular flow." International Journal of Multiphase Flow, 17(4), 455-468.

[19] Spalart, P. and Allmaras, S., 1992, "A one-equation turbulence model for aerodynamic flows." American Institute of Aeronautics and Astronautics.

[20] Manninen, M., Taivassalo, V., and Kallio, S., 1996, "On the mixture model for multiphase flow." VTT Publications 288, Technical Research Centre of Finland, Finland.